AGU PUBLICATIONS

Water Resources Research

RESEARCH ARTICLE
10.1002/2016WR019875

Key Points:
- Hyporheic flow path geometry varies with discharge, even in cases where transport times remain unchanged
- In-stream discharge and along-stream morphology cannot be used to identify flow path origination locations
- Observations of solute tracers have a spatial window of detection in addition to the more broadly recognized temporal window of detection

Supporting Information:
- Supporting Information S1

Correspondence to:
A. S. Ward,
adamward@indiana.edu

Citation:
Ward, A. S., N. M. Schmadel, S. M. Wondzell, M. N. Gooseff, and K. Singha (2017), Dynamic hyporheic and riparian flow path geometry through base flow recession in two headwater mountain stream corridors, *Water Resour. Res.*, *53*, doi:10.1002/2016WR019875.

Received 30 SEP 2016
Accepted 19 APR 2017
Accepted article online 26 APR 2017

Dynamic hyporheic and riparian flow path geometry through base flow recession in two headwater mountain stream corridors

Adam S. Ward[1], Noah M. Schmadel[1], Steven M. Wondzell[2], Michael N. Gooseff[3], and Kamini Singha[4]

[1]School of Public and Environmental Affairs, Indiana University, Bloomington, Indiana, USA, [2]Pacific Northwest Research Station, United States Department of Agriculture, Forest Service, Corvallis, Oregon, USA, [3]Institute of Arctic and Alpine Research, University of Colorado, Boulder, Colorado, USA, [4]Hydrologic Science and Engineering Program, Colorado School of Mines, Golden, Colorado, USA

Abstract The hydrologic connectivity between streams and their valley bottoms (stream corridor) is a critical determinant of their ecological function. Ecological functions are known to be spatially and temporally variable, but spatial dimensions of the problem are not easily quantified and thus they are usually overlooked. To estimate the spatial patterns of connectivity, and how connectivity varies with changes in discharge, we developed the hyporheic potential model. We used the model to interpret a series of solute tracer injections in two headwater mountain streams with contrasting valley bottom morphologies to estimate connectivity in the stream corridor. The distributions of flow path origination locations and the lengths of hyporheic flow paths appear to vary with base flow recession, even in cases where transport timescales are apparently unchanged. The modeled distribution of origination locations further allowed us to define a spatial analog to the temporal window of detection associated with solute tracer studies, and enables assessment of connectivity dynamics between streams and their corridors. Altogether, the reduced complexity hyporheic potential model provides an easy way to anticipate the spatial distribution and origination locations of hyporheic flow paths from a basic understanding of the valley bottom characteristics and solute transport timescales.

Plain Language Summary The manuscript details a simple method to assess the spatial connectivity of streams and their riparian zones. While the timescales of exchange in the river corridor have been broadly studied, the complimentary spatial dimension (i.e., the geometry of exchange flowpaths) remains largely unknown. The major challenge in assessing the spatial dimensions of exchange is the limited information available in the subsurface. Here, we develop a reduced complexity model of valley bottom transport to overcome these information limitations. With this model, relatively simple field site characterization and solute tracer data are combined to assess the spatial distribution of downwelling along a headwater mountain stream. We validate the model with a numerical experiment, and demonstrate its application in two watersheds of contrasting geology, repeated through baseflow recession.

1. Introduction

Accurate representation of hydrologic connectivity between streams and their aquifers (i.e., the "stream corridor" [*Harvey and Gooseff*, 2015]) is fundamental to understanding biogeochemical processes and other ecosystem functions [e.g., *Stanford and Ward*, 1993; *FISRWG*, 1998]. This connectivity is controlled by different, interactive elements of the stream corridor including valley setting (geologic control) and dynamic hydrologic forcing (hydrologic control). For this study, we define connectivity on the basis of a flow path originating in the stream and intersecting another at a location of interest (e.g., a riparian well). To date, connectivity has been broadly described as a binary characteristic—elements are either connected or not [*Jencso et al.*, 2009, 2010; *Jencso and McGlynn*, 2011; *Pringle*, 2003; *Bracken and Croke*, 2007; *Tetzlaff et al.*, 2007; *Blume and Van Meerveld*, 2015; *Wainwright et al.*, 2011]. Much research has emphasized the timescale of connectivity as a key determinant of ecological function [e.g., *Ward et al.*, 2011; *Gooseff*, 2010; *Bencala*, 2011]. Here we stress that the spatial

distribution in the stream corridor is a critical control to determining the physical, chemical, and biological functions associated with exchange flow paths [e.g., *Cardenas*, 2008a, 2008b; *Harms and Grimm*, 2008; *McGuire and McDonnell*, 2010; *Ocampo et al*., 2006; *Ward et al*., 2011]. Only by accounting for both the timescales and spatial geometry of hydrologic connectivity, accurate predictions of these functions can be made.

Most stream corridor studies to date have focused on hyporheic flow path timescales as a control on biogeochemical processes. In contrast, the geometry of these same subsurface flow paths remains virtually unknown, despite recognition that spatial heterogeneity (commonly "patchiness") is a critical determinant of ecological functions. Flow path geometry may include descriptors such as the length of hyporheic flow paths, their origination point from the stream, direction of flow, and tortuosity. The absence of predictive power in flow path geometry limits our ability to make meaningful predictions of stream corridor functions. Therefore, we seek to characterize flow path geometry (primarily the location of flow path origination from the stream) and transit time as a function of geologic controls and dynamic hydrologic forcing, both of which are recognized as controls on stream corridor exchange [*Wondzell et al*., 2009; *Ward et al*., 2012, 2016; *Wondzell and Gooseff*, 2013; *Boano et al*., 2014]. By characterizing both flow path geometry and transit time, we seek to describe spatially heterogeneous and temporally dynamic connectivity between streams and their corridors. Furthermore, the combination of spatial and temporal data enables assessment of connectivity with a richer characterization than a binary definition of connected or not.

Attempts to characterize hyporheic flow path geometry in the field are limited due to the difficulty of making subsurface observations. The most common approach to assess flow path geometry uses extensive networks of monitoring wells [e.g., *Wroblicky et al*., 1998; *Wondzell and Swanson*, 1999; *Zarnetske et al*., 2012]. Water table shape derived from such networks has been used to estimate flow path geometry [e.g., *Kasahara and Wondzell*, 2003; *Voltz et al*., 2013], though estimates from this approach commonly lack independent field validation. Downwell tracer injections in monitoring well networks have been used to measure individual hyporheic flow paths [e.g., *Zarnetske et al*., 2012; *Menichino et al*., 2014]. Monitoring well observations provide a basis to calibrate or validate distributed hydrogeological models [e.g., *Wondzell et al*., 2009; *Ward et al*., 2013b]. Such modeling approaches, however, are beset by challenges in parameterizing the hydraulic conductivity field, where parameter equifinality prevents identifying a unique solution [e.g., *Beven*, 1993, 2006; *Cardenas and Zlotnik*, 2003]. Likewise, the locations where flow paths originate (hereafter origination locations or OLs) and the spatial extent of flow paths are often unknown. As a result, the ability of modeling approaches to accurately predict flow path-scale geometry and transit time has been the subject of much debate [e.g., *Oreskes et al*., 1994; *Poeter*, 2007; *Wondzell et al*., 2009]. Consequently, the OLs of flow paths and their subsurface geometry within the stream corridor remain poorly characterized. Without this information, management of the stream corridor that considers these ecologically important exchange processes will remain infeasible or inaccurate.

While recent work in mountain streams demonstrates that connections between streams and their stream corridors persist through base flow recession [e.g., *Wondzell*, 2006; *Voltz et al*., 2013; *Ward et al*., 2016; *Payn et al*., 2009, 2012], it remains unknown how the nature of this connectivity changes in both space and through time. Therefore, our study has two primary objectives: (1) to derive and validate a reduced complexity model to describe flow path geometry in the riparian zone of headwater mountain streams and (2) to apply our reduced complexity model to interpret flow path geometry and spatial connectivity during a field experiment. First, we derive a reduced complexity model to predict flow path origination point and validate the model by comparing predictions to a finite element model representative of the field site. Next, we use the reduced complexity model to interpret a series of stream solute tracer studies conducted in two valleys of contrasting morphology to identify the locations along the stream where observed riparian flow paths were likely to originate and to assess changes in flow path geometry and the field site through base flow recession. We hypothesize that hyporheic flow path geometry at this site will remain stable through base flow recession given previous findings that many transport timescales are static through the season [*Ward et al*., 2016], and the observed static morphology of the system. Additionally, we anticipate that distinct in-channel features such as pool-riffle-step sequences will be focused locations for flow path origination that persist through base flow recession.

2. Derivation of the Hyporheic Potential Model

Here we propose a reduced complexity model—the hyporheic potential model—to estimate OLs along a stream on the basis of simple geometric observations, observed transport timescales, and aquifer properties.

2.1. Simplified Geometry of the Stream-Hyporheic System

First, the geometry is represented as in-stream transport occurring linearly in the down-valley direction and hyporheic transport described by both down-valley and cross-valley components of transport (Figure 1a). Consider a particle traveling from a solute tracer injection location to a subsurface monitoring well; the approximate geometry of the associated flow path can be defined as,

$$L = L_{STR} + L_{HZDV} \tag{1}$$

$$L_{HZ}^2 = L_{HZDV}^2 + L_{HZCV}^2 \tag{2}$$

where L is the total down-valley length from the injection location to the monitoring well, L_{STR} is the in-stream down-valley transport, L_{HZ} is the total length of transport in the hyporheic zone, and L_{HZDV} and L_{HZCV} represent the down-valley and cross-valley components of hyporheic transport, respectively. This formulation assumes that transport in the vertical dimension is negligible compared to cross-valley and down-valley transport.

2.2. Transport Timescales From Experimental Solute Tracer Additions

Consider a solute tracer injection conducted in the stream at a distance L upstream of the monitoring well. The mean arrival time observed at the well (t_{OBS}) represents the sum of travel time in the stream (t_{STR}) and hyporheic zone (t_{HZ}),

$$t_{OBS} = t_{STR} + t_{HZ}. \tag{3}$$

In this model, the first temporal moment (M_1) of an observed solute tracer time series represents t_{obs}. To estimate transit timescales to each well, we subtract the first temporal moment of the injected solute tracer

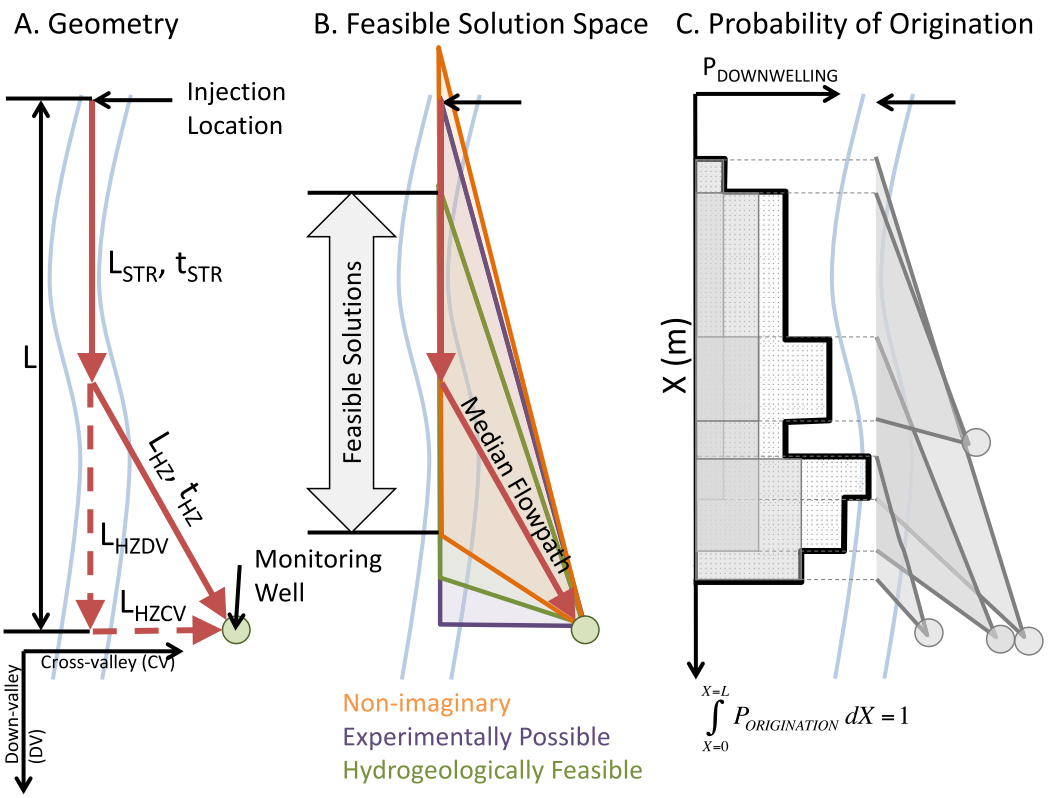

Figure 1. (a) Idealized stream and hyporheic flow path geometry in the valley bottom. (b) The feasible solution space is bounded by the overlapping range of solutions that are nonimaginary, originate between the injection location and well transect (experimentally possible), and are hydrogeologically feasible given the known range of K, θ, and S at the site. (c) For cases with multiple wells—for example, the four shown in this figure—the feasible solutions for each well are summed and then normalized along the stream. The result is a probability distribution of flow path origination as a function of distance along the stream channel.

time series in the stream from the first temporal moment calculated from observations at the monitoring well [after *Ward et al.*, 2014, 2016].

2.3. Estimation of Advective Velocities From Experimental and Site Data

The transit times in the stream and hyporheic zone can be represented as the ratio of their length scale to velocity,

$$t_{STR} = \frac{L_{STR}}{V_{STR}}, \tag{4}$$

$$t_{HZ} = \frac{L_{HZ}}{V_{HZ}}, \tag{5}$$

where V_{STR} and V_{HZ} are the stream and hyporheic zone velocities, respectively. In-stream velocity was estimated as the difference between observed in-stream M_1 at the injection site and the downstream-most well transect, divided by the length of the stream channel (L) [after *Ward et al.*, 2014].

Subsurface velocity is estimated using Darcy's law as follows:

$$V_{HZ} = \frac{K}{\theta}\frac{dh}{dL}, \tag{6}$$

where K is isotropic hydraulic conductivity, θ is effective porosity, dh is the head drop along the hyporheic flow path, and dL is the length of the hyporheic flow path (equal, here, to L_{HZ}). The head drop along the hyporheic flow path must be equal to the sum of cross-valley and down-valley head drops,

$$dh = dh_{CV} + dh_{DV}. \tag{7}$$

Substitutions of equations (4–7) into equation (3) yields,

$$t_{OBS} = \frac{L_{STR}}{V_{STR}} + \frac{L_{HZ}}{\frac{K}{\theta} \times \frac{dh_{CV}+dh_{DV}}{L_{HZ}}}. \tag{8}$$

Equation (8) represents the general form of the Hyporheic Potential Model (HPM). One important assumption of this formulation is that the time spent in the stream channel is based on the advective timescale along the stream. Thus, any time spent in nonadvective transport (e.g., temporary storage in recirculating eddies and boundary layers) is effectively assigned to transport through the subsurface. Additionally, the formulation assumes that flow paths remain in the stream until their origination point; the solution does not include the impact of repeated spiraling between the stream and riparian zone. This isolation of only the last exchange is analogous to hydrologic turnover formulations, which acknowledge spiraling but focus only on the last exchange [*Covino et al.*, 2011].

2.4. Simplification of the Hyporheic Potential Model for the Field Site

At the study site, the system is dominated by down-valley subsurface transport [*Voltz et al.*, 2013]. On this basis, we assume $dh_{DV} \gg dh_{CV}$ (i.e., $dh_{CV} \approx 0$). Furthermore, down-valley head gradients can be approximated by the down-valley topographic gradient [e.g., *Voltz et al.*, 2013; *Ward et al.*, 2014, 2016], itself set by the geology and morphology of the valley bottom. On this basis, the down-valley head drop can be approximated as,

$$dh_{DV} = L_{HZDV} S, \tag{9}$$

where S is the down-valley topographic gradient. Thus, equation (8) may be simplified to,

$$t_{OBS} = \frac{L_{STR}}{V_{STR}} + \frac{\theta}{KS}\frac{L_{HZ}^2}{L_{HZDV}}. \tag{10}$$

Notably, the quantity KS is referred to as "hyporheic potential" by *Wondzell* [2011], the namesake of this model.

2.5. Constraining Solutions for the Hyporheic Potential Model at a Field Site

The quantities L and L_{HZCV} are readily observed using topographic surveys or measurements of the field site. Common solute tracer studies provide information about t_{OBS} and V_{STR}, assuming observations are

made at two stream locations and in a riparian well. If values of K, θ, and S can be estimated from a field site, equations (1), (2), and (10) can be solved for the remaining unknowns of L_{HZDV}, L_{HZ}, and L_{STR}. To be considered a feasible solution (i.e., a location where a flow path may have feasibly originated), three conditions must be met (Figure 1b). First, a nonimaginary solution to equations (1–3) must exist. Next, the flow path must be experimentally possible, with flow path origination predicted between the injection location and well transect. Finally, the solution must be hydrogeologically feasible, meaning that it is within the suite of flow paths constrained by the ranges of site-specific θ, K, and S.

2.6. Interpretation of Hyporheic Potential Model Results

The median location of the estimated flow path distribution is used to assess changes in flow path origination through base flow recession, visualized as the middle of the "wedge" of feasible solutions shown in Figure 1b. With estimates of L_{STR}, L_{HZ}, and L_{HZDV}, we additionally calculated the fractional length in the HZ ($F_{LHZ} = L_{HZ}/L$), time in HZ ($t_{HZ} = L_{HZ}/(KS/\theta^{*}L_{HZDV}/L_{HZ})$, time in stream ($t_{STR} = L_{STR}/V_{STR}$), and the fraction of time in HZ ($F_{tHZ} = t_{HZ}/t_{obs}$). Finally, we assigned equal probability to origination location within the range of feasible flow paths for each well (Figure 1b). At our field sites, the same tracer injection was monitored at a network of shallow subsurface monitoring wells. The probabilities for origination location for all wells were summed along the steam and normalized by the number of wells, resulting in a probability density function describing the potential locations where flow paths originate from the stream (for example, Figure 1c depicts a case with four monitoring wells).

3. Validation of the Hyporheic Potential Model Using Numerical Experiments

3.1. Methods

To validate the HPM, we test its performance in accurately predicting the OLs of flow paths using a series of numerical experiments. We constructed a 2-D, vertically integrated (i.e., plan view) finite element model of groundwater transport through the hyporheic and riparian zone adjacent to a stream channel (Figure 2a),

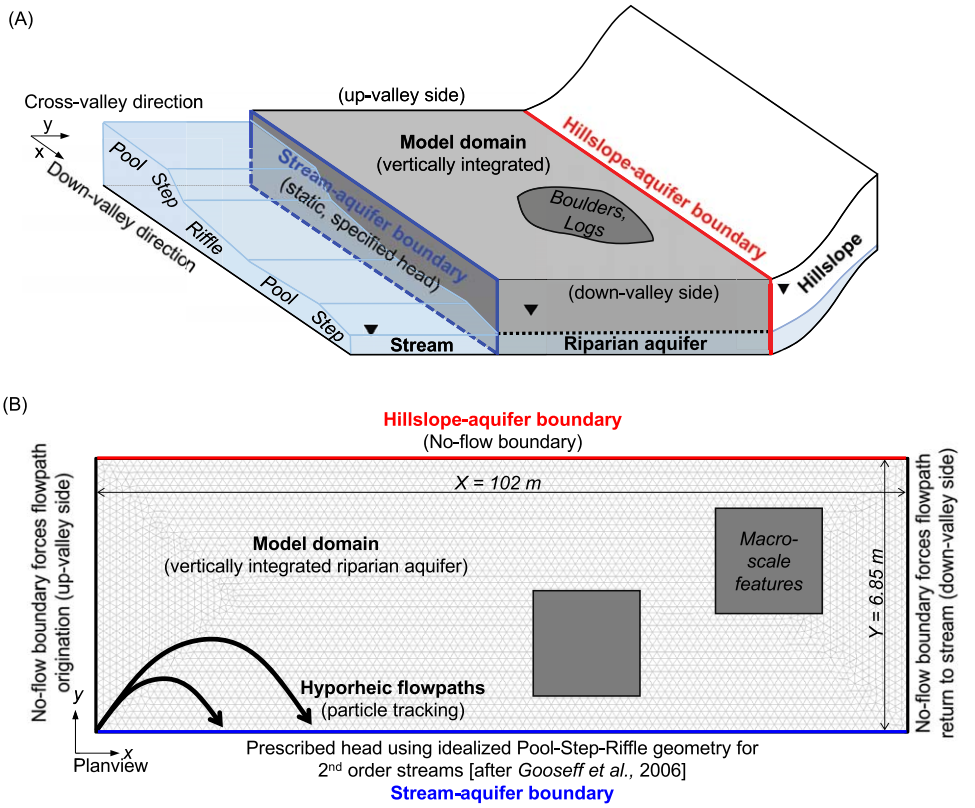

Figure 2. (a) Conceptual model of a riparian aquifer bounded by the stream and hillslope in longitudinal dimensions. (b) Implementation of a vertically integrated (i.e., plan view) mathematical model of the riparian aquifer. Modified from *Schmadel et al.* [2016] with permission.

following similar model construction of past studies of hyporheic and riparian zones in COMSOL Multiphysics [*Schmadel et al*., 2016; *Malzone et al*., 2016; *Ward et al*., 2011]. The model domain was set to mimic the conditions of our field site in WS01 at the H.J. Andrews Experimental Forest, including an average riparian zone width of 6.85 m from stream centerline to valley edge. In the field, unweathered bedrock is present below about 2 m of colluvium (Figure 2b).

We parameterized the subsurface hydraulic conductivity field with random values drawn from a normal distribution in log-space with a mean of 7×10^{-5} m s^{-1} (matching the geometric mean of on-site observations [*Kasahara and Wondzell*, 2003; *Wondzell et al*., 2009]) and standard deviation of $10^{0.4}$ m s^{-1}. Observations at the field site range from 4.3×10^{-6} to 6.1×10^{-4} m s^{-1} [*Kasahara and Wondzell*, 2003; *Wondzell et al*., 2009]. For the numerical model we assumed a homogeneous porosity of 0.2 for the entire domain. Additionally, we represented macroscale features to approximate the large boulders and coarse woody debris at the field site, simulated as 2 m squares with hydraulic conductivity of 1×10^{-20} m s^{-1}.

The model includes no-flow boundaries along three boundaries and prescribed head along the fourth, representing the boundary between the riparian zone and stream. We use the no-flow boundaries at the upstream and downstream ends of the domain to force the formation of a hyporheic flow cell in the model domain [after *Irvine et al*., 2015; *Irvine and Lautz*, 2015, Figure 3]. At the field site, these types of boundaries are representative of visible outcrops of bedrock where the valley narrows and most water is returned to the surface stream channel before subsequent return to the subsurface. The no-flow boundary along the hillslope represents an assumption that lateral inflows to the valley bottom are negligible along the study reach.

The prescribed head along the stream decreases along the model in the x dimension from an assumed elevation of 100 m at X = 0. Head was set using the idealized second-order stream geometry for a pool-step-riffle morphology reported by *Gooseff et al*. [2006] for the H.J. Andrews Experimental Forest. We repeated

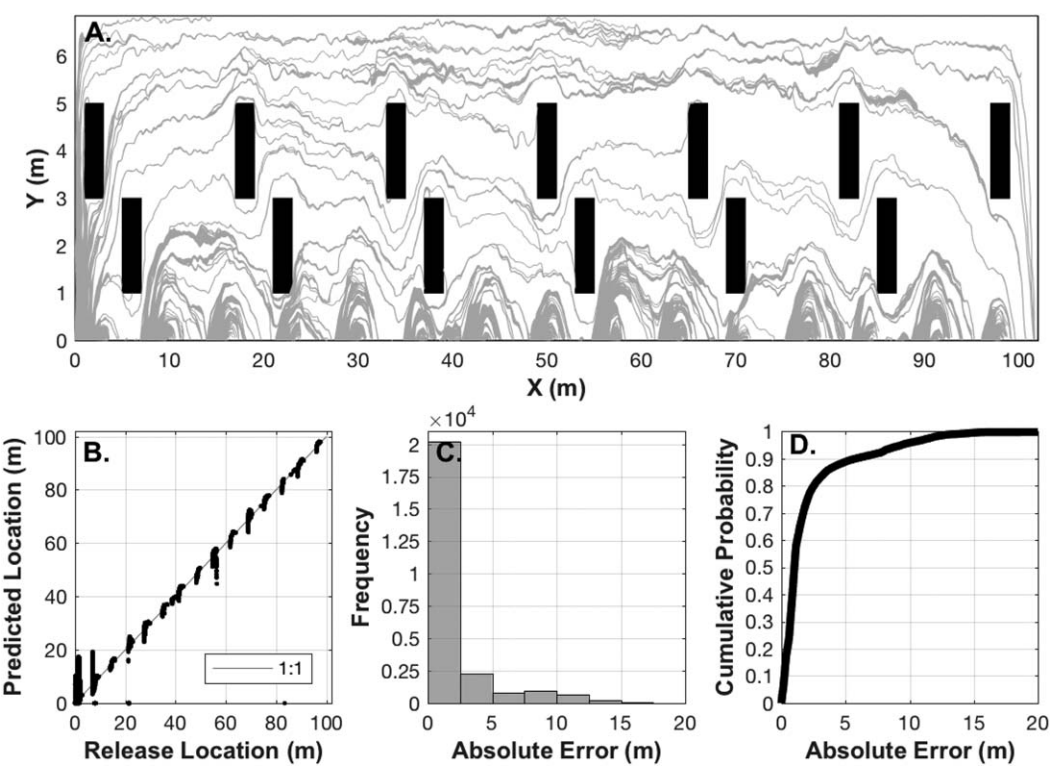

Figure 3. (a) Representative particle tracks from release of massless particles at 1 cm intervals along the Y = 0 m boundary. The hyporheic potential model was used to predict the downwelling location for each particle based on the time when it passed each 1 m along the stream. The white field is a random hydraulic conductivity field; black rectangles represent low conductivity discontinuities such as boulders or logs in the domain. (b) Known release location (*x* axis) versus hyporheic potential model predicted location (*y* axis) for all particle-transect intersects. (c) Histogram of error for each hyporheic potential model prediction. (d) Cumulative distribution of error in hyporheic potential model predictions for particles.

15 sequences of the idealized pool (2.1 m length, 0 m elevation drop), step (1.4 m length, 0.4 m elevation drop), and riffle (3.3 m length, 0.2 m head drop) morphology for a total down-valley length of 102 m in the X dimension. This morphology represents an average down-valley gradient of about 8.8%.

For each simulation, a triangular mesh (finite element) was constructed using the built-in meshing algorithm in COMSOL Multiphysics v.5.0 for general physics application with a maximum mesh size of 0.25 m^2. The resultant mesh contained 7610 elements with an average element size of about 0.09 m^2 and average element quality (a measure of element asymmetry) of 0.98. First, the porous media flow simulation was solved to a steady state solution. Next, we released 10,200 massless particles along the constant head boundary (1 particle per cm in the X dimension along the Y = 0 m boundary). Particle positions were recorded every 3600 s until they exited the model domain by flowing from the simulated subsurface domain across the stream boundary.

We applied the HPM to the simulated particle paths to test how well the OLs were predicted relative to the known release locations in the finite element model. We tabulated the known time and cross-valley coordinate (i.e., Y coordinate) for each particle as it crossed each 1 m along the X dimension of the model (representing hypothetical monitoring well transects at each of these locations). For each time and location where a particle passed a transect, we used the HPM to calculate the OL for the particle. First, we calculated the absolute error in the OL inferred from the HPM using the prescribed mean hydraulic conductivity, porosity, and average down-valley hydraulic gradient for the model domain. Next, we calculated the feasible range of OLs based on the range of hydraulic conductivity values assigned and the prescribed porosity and average down-valley slope. This scenario approximates the conditions faced by field researchers, where estimation of transit timescales and flow path geometries are desired even acknowledging the uncertainty in hydrogeologic parameters.

For each particle, and at each transect, we calculated the feasible range to test whether true OL was within the range predicted by the HPM. Error in the predicted OL was calculated as the distance between the known and predicted locations as $X_{pred} - X_{obs}$, where X_{pred} and X_{obs} are the HPM-predicted and observed OLs, respectively. Values less than zero indicate predicted origination occurred upstream (i.e., the negative X direction) of the known location. Finally, we calculated the sinuosity of each particle's flow path at the time it crossed the monitoring transect. This calculation was made by dividing the length of the particle's path (based on the recorded positions of the particle) by the straight-line distance from the release location to the location where the particle crossed the transect of interest.

3.2. Results and Discussion

Particle flow paths show the deepest penetration of flow paths into the subsurface domain in the first few meters in the X dimension due to the no-flow boundary at X = 0 m. The pool-step-riffle and macroscale heterogeneities interact to cause a series of smaller, nested flow cells along the Y = 0 m model boundary. Heterogeniety in the hydraulic conductivity field is visible in the tortuosity along the flow paths (Figure 3a).

Hyporheic potential model predictions of OL are highly accurate (Figures 3b and 3c). A total of 23,362 predictions were made, with a mean absolute error of about 2.1 m and median absolute error of about 1.0 m. About 91% of model predictions are within 6.8 m of the true OL, meaning the correct pool-step-riffle sequence can be accurately identified using the HPM (Figure 3d).

Overall, we conclude that the HPM provides reasonable predictions of the OLs of flow paths in steep, valley-constrained stream corridors. The largest limitation of the model appears to be the sinuosity of flow paths. Sinuosity violates two key model assumptions. First, the HPM assumes transport along the hypotenuse of a right triangle. The added flow path length due to sinuosity causes the HPM to systematically predict origination farther upstream than would be expected. Second, the cross-valley transport occurring along sinuous flow paths reduced the effective hydraulic gradient along the flow path. The HPM assumes that the down-valley slope is the primary driver of riparian zone transport. Flow paths with large cross-valley transport relative to their down-valley transport exhibit larger errors. Despite these violations of HPM assumptions, the HPM accurately predicted the OL for most flow paths. Furthermore, uncertainty in the parameters controlling subsurface velocity (S, K, and θ) is large enough that the predicted ranges of OL encompassed the true flow path origin in all cases.

4. Dynamics of Flow Path Geometry Through Base Flow Recession in Two Headwater Mountain Streams of Contrasting Geologic Setting

4.1. Field Site and Experimental Design

Field experiments were conducted in Watersheds 1 (WS01) and 3 (WS03) of the H.J. Andrews Experimental Forest in the Cascade Mountains, Oregon, USA (supporting information Figure S1). Both catchments are characterized by steep valley walls and average down-valley slopes of 11.9 and 13.8% in WS01 and WS03, respectively. Valley bottom transport is known to be predominantly in the down-valley direction [*Voltz et al*., 2013; *Kasahara and Wondzell*, 2003], making this a strong candidate site to apply the HPM. Valley bottoms in WS01 are about 3.5 active channel widths (∼14 m) compared to 2.3 active channel widths (∼9 m) in WS03 [*Wondzell*, 2006]. Both field sites are confined by shallow bedrock, with typically less than 2 m of highly porous colluvium in the valley bottom. In WS01, a network of 33 wells and 7 in-stream monitoring piezometers were installed; WS03 contained 19 wells and 7 in-stream piezometers. At these sites, the stream corridor is equivalent to the entire valley bottom. The stream corridor includes the stream itself, the hyporheic zone, and the riparian zone. See additional publications for general characteristics of the study site [*Dyrness*, 1969; *Swanson and James*, 1975; *Swanson and Jones*, 2002], construction of the monitoring well network [*Wondzell*, 2006], and detailed characteristics of the study site [*Kasahara and Wondzell*, 2003; *Wondzell et al*., 2009; *Ward et al*., 2012, 2016; *Voltz et al*., 2013].

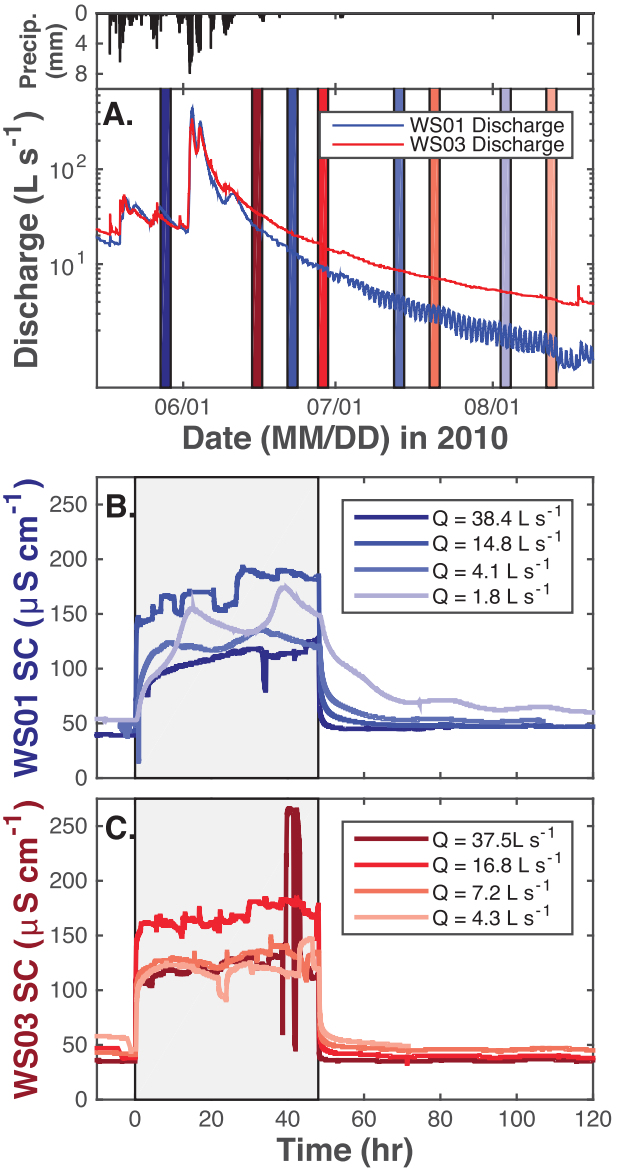

Figure 4. (a) Hyetograph and hydrographs for the study watersheds, and the time periods for the eight constant-rate injections included in the study. Figures 4b and 4c show the observed in-stream-specific conductance at the upstream end of the well transect for each injection in Watersheds 1 (WS01) and 3 (WS03). Reprinted with permission from *Ward et al*. [2016].

We conducted a series of four 48 h constant rate solute tracer (salt as NaCl) injections into the stream channel throughout base flow recession in each watershed and monitored specific conductance at the in-stream locations and in each monitoring well. Stream discharge during our study ranged from 38.5 to 1.8 L s^{-1} in WS01, and from 37.5 to 4.3 L s^{-1} in WS03, recorded at gage stations about 100 m downstream of the study well networks (Figure 4a). Observed solute tracer time series were processed identically to *Ward et al*. [2016], calculating the first temporal moment (M_1) for each background-corrected time series and subtracting the first temporal moment of the injection at the upstream reach limit, yielding the observed mean arrival time of the tracer at each monitoring point (taken as t_{obs} in equation (3)) [after *Ward et al*., 2016]. During the four stream solute tracer injections in each watershed, in-stream-specific conductance was increased to plateau concentrations ranging from about 110 to 190 μS cm^{-1} at the upstream end of the monitoring well

network (Figures 3b and 3c and supporting information Figure S2). Transit times from the injection location to well transect C ranged from 0.18 to 1.18 h in WS01 and 0.08 to 0.34 h in WS03. Observed mean arrival times at monitoring wells ranged from 27.9 to 126.4 h in WS01 and from 30.4 to 82.1 h in WS03 (supporting information Figure S2). Several related publications present additional details of catchment hydrology and hydraulics during the study period [*Voltz et al*., 2013], and the conservative solute tracer injections and monitoring [*Ward et al*., 2012, 2014, 2016; *Voltz et al*., 2013].

For this study, the geometry of the study site (i.e., injection location and well layout) defines the values of L and L_{HZCV} (cross-valley distance from the stream to the well). Field solute tracer observations may be used as the basis to calculate t_{OBS} and V_{STR}. Using observed ranges for the site to constrain values of K, θ, and S, equations (1–3) represent a system with three unknown variables (L_{STR}, L_{HZ}, and L_{HZDV}). A range of feasible solutions for these three unknowns was calculated given the observed ranges in K (4.3×10^{-6} to 6.1×10^{-4} m s^{-1} [*Kasahara and Wondzell*, 2003; *Wondzell et al*., 2009], θ (0.1–0.3 [*Wondzell et al*., 2009; *Ward et al*., 2012]), and S (0.06–0.16 mm^{-1}; topographic survey) at the field site (see subsequent section).

To test for differences between sites in WS01 and WS03 or between discharge conditions at the same site, we analyze the sets of observed transit times and calculated L_{HZ}, L_{STR}, t_{HZ}, t_{STR}, F_{LHZ}, and F_{tHZ} for each discharge condition and site. We apply the one-way analysis of variance and Kruskal-Wallis one-way analysis of variance by ranks to test for significant differences in sample means (denoted by p_{ANOVA}) or medians (denoted by p_{KW}), respectively. For this study, we interpret significance at the 95% confidence level ($p < 0.05$). Finally, we use a two-sample Kolmogorov-Smirnov goodness-of-fit hypothesis test to determine if continuous distributions of flow path origination probability are significantly different from one another.

4.2. Results

4.2.1. Variation in Flow Path Geometry and Transport Timescales Through Base Flow Recession

4.2.1.1. Length of Transport in the Hyporheic Zone

Across all injections, L_{HZ} ranged from 0.27 to 58 m in WS01 and 0.25 to 28 m in WS03 (Figure 4a and supporting information Figure S3). Stream discharge is not consistently related to L_{HZ} in the less constrained WS01 ($\Delta L_{HZ}/\Delta Q < 0$ for 17 of 33 wells; $\Delta L_{HZ}/\Delta Q > 0$ for 16 of 33 wells). Most wells in the more constrained WS03 exhibit increasing L_{HZ} under lower-discharge conditions ($\Delta L_{HZ}/\Delta Q < 0$ for 16 of 19 wells). Within WS01, we calculated significant differences in L_{HZ} populations between discharge conditions ($p_{ANOVA} < 0.001$, $p_{KW} < 0.001$), but no significant differences between discharge conditions for WS03 ($p_{ANOVA} = 0.09$, $p_{KW} = 0.15$). We calculated significant differences in L_{HZ} between the populations of wells in WS01 and WS03 for injections 2 and 4 (p_{ANOVA}, $p_{KW} < 0.01$), but not for injections 1 and 3 in WS01 ($p_{ANOVA} = 0.65$, $p_{KW} = 0.60$) nor WS03 ($p_{ANOVA} = 0.12$, $p_{KW} = 0.16$).

4.2.1.2. Fraction of Total Length in the Hyporheic Zone

In-stream transport is generally longer in spatial scale than transport along hyporheic flow paths (Figures 4b and 4c and supporting information Figures S4 and S5). We found 74% of well observations in WS01 (90 of 121) and 96% in WS03 (71 of 74) where $L_{STR} > L_{HZ}$. We found that the fraction of length in the hyporheic zone (F_{LHZ}) ranges from 1 to 99% in WS01 and 0 to 60% in WS03. Overall, F_{LHZ} was larger in the broader alluvial valley, with mean and median F_{LHZ} of 37 and 32% in WS01, compared to 18 and 15% in the more constrained WS03. Valley morphology is a significant control on F_{LHZ} under intermediate and low-discharge conditions, with significant differences between the WS01 and WS03 for injections 2–4 ($p_{ANOVA} < 0.05$, $p_{KW} < 0.05$). Under the highest discharge conditions, we found $p_{ANOVA} = 0.31$ and $p_{KW} = 0.40$, which we interpret as the dominance of in-stream advection in both study sites compared to subsurface transport controlled by valley structure.

With respect to discharge as a control on F_{LHZ} within each watershed, we calculated significant differences between discharge conditions in WS01 (p_{ANOVA}, $p_{KW} < 0.001$) but not in WS03 ($p_{ANOVA} = 0.07$, $p_{KW} = 0.16$). In WS01, 31 of 33 wells exhibited an inverse relationship between F_{LHZ} and discharge, and the heterogeneity in observed values increases with decreasing discharge. In WS03 the inverse relationship between discharge and F_{Lhz} exists for 15 of 19 wells. In WS01, increasing discharge is associated with decreased F_{LHZ} for injections 1 and 4, and increased F_{LHZ} for injections 2 and 3.

4.2.1.3. Transport Time in the Hyporheic Zone

Transport time in the hyporheic zone (t_{HZ}) ranged from 1.7 to 102.7 h in WS01 and 5.7 to 56.6 h in WS03 (Figure 4d and supporting information Figure S6). In WS01, significant differences (p_{ANOVA}, $p_{KW} < 0.001$) were observed between discharge conditions, primarily with significantly longer t_{HZ} during injection 4

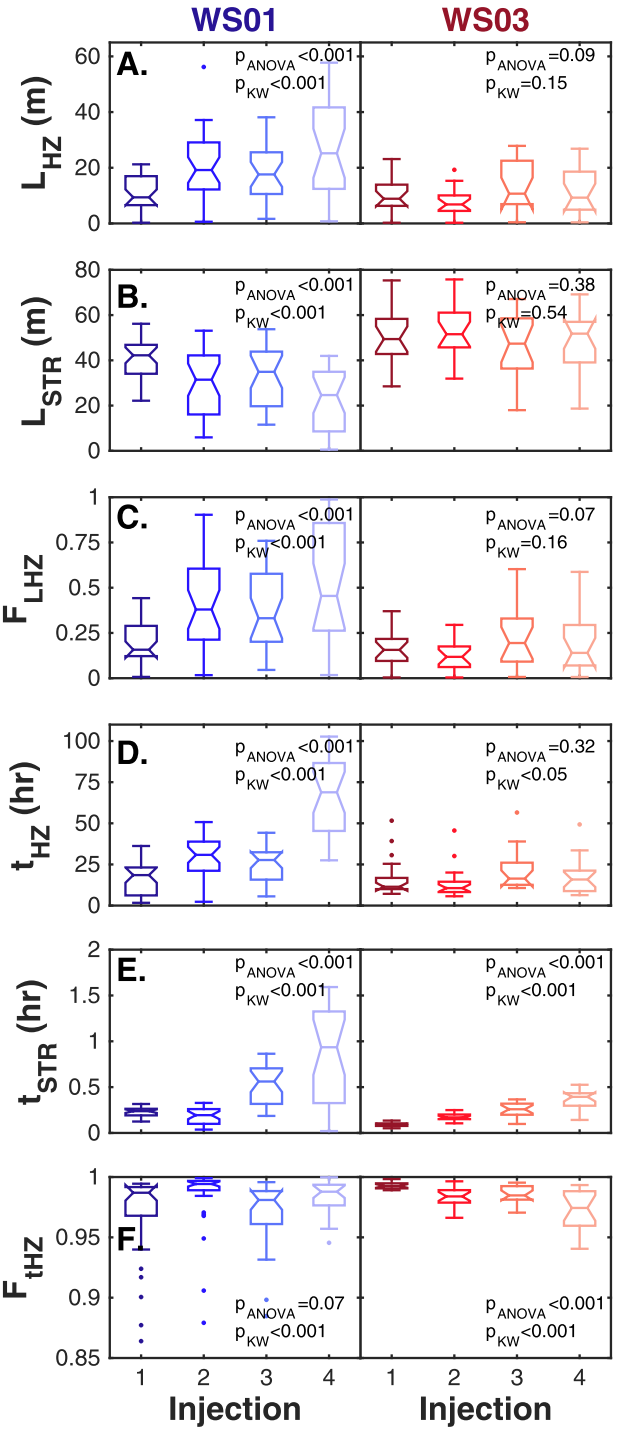

Figure 5. Summary of flow path-scale metrics describing (a) length of hyporheic transport (L_{HZ}), (b) length of in-stream advective transport (L_{STR}), (c) fraction of total length in hyporheic zone (F_{LHZ}), (d) transit time in the hyporheic zone (t_{HZ}), (e) transit time in the stream (t_{STR}), and (f) fraction of transit time in the hyporheic zone (F_{tHZ}). For each set of injections, results of one-way ANOVA and Kruskal-Wallis tests are presented to assess if at least one flow condition is significantly different from the others for each watershed.

compared to injections 1–3. In WS03, differences between discharge conditions were significant for t_{HZ} medians but not means ($p_{ANOVA} = 0.32$, $p_{KW} = 0.046$). Significant differences for t_{HZ} exist between watersheds for injections 2 (p_{ANOVA}, $p_{KW} < 0.001$) and 4 (p_{ANOVA}, $p_{KW} < 0.001$), but not for injections 1 ($p_{ANOVA} = 0.97$, $p_{KW} = 0.64$) or 3 ($p_{ANOVA} = 0.24$, $p_{KW} = 0.11$).

We calculated increasing t_{HZ} with decreasing discharge for 28 of 33 wells in WS01 and 4 of 19 wells in WS03. These results are in good agreement with *Ward et al.* [2016] who concluded hyporheic transit times were generally constant through base flow recession in WS03 across all injections and for injections 1–3 in WS01.

4.2.1.4. Fraction of Total Time in the Hyporheic Zone

Although hyporheic flow paths did not represent a majority of the transport length from the injection location to the monitoring wells, they always represented a majority of the time in transport (Figures 4e and 4f and supporting information Figures S7 and S8). We found F_{tHZ} ranged from 86 to 100% in WS01 and from 94 to 100% in WS03. Despite orders of magnitude variation in K, median F_{tHZ} is strikingly uniform among all wells. Differences between injections were significant in WS01 for medians but not means ($p_{ANOVA} = 0.067$, $p_{KW} < 0.001$) and significant for both mean and median in WS03 (p_{ANOVA}, $p_{KW} < 0.001$). For a given base flow condition, significant differences between watersheds were found for injections 1 (p_{ANOVA}, $p_{KW} < 0.001$) and 4 ($p_{ANOVA} = 0.025$, $p_{KW} = 0.026$). Differences between watersheds were significant for mean but not median for injection 3 ($p_{ANOVA} = 0.034$, $p_{KW} = 0.062$) and medians but not means for injection 2 ($p_{ANOVA} = 0.88$, $p_{KW} = 0.002$). We calculated increasing F_{tHZ} with discharge in 20 of 33 wells in WS01 and only 1 of 19 wells in WS03.

4.2.2. Spatial Distribution of Flow Path Origination Locations

In WS01, flow path origination along the stream ranged from $X = 0$ to 61.5, 0 to 61.4, 0 to 58.7, and 0 to 51.7 m for injections 1–4, respectively (X is distance downstream from the injection; Figure 6a). In WS03, flow path origination ranged from $X = 0$ to 78.1, 10.2 to 78.7, 0 to 71.0, and 0 to 72.3 m

for injections 1–4, respectively (Figure 6b). In both watersheds, there is a general trend of the mean origination location shifting upstream as base flow decreases. In WS01, the probability of flow path origination upstream of the well network increased from 42% during injection 1 to 92% during injection 4 (Figure 6c), and is negatively skewed in space for injections 1–3 and positively skewed for injection 4. The probability of flow path origination upstream of the well network in WS03 ranges from 59 to 77%, with a trend of flow paths generally originating closer to the injection location with decreasing discharge (Figure 6d). In WS03, the cumulative distribution function is positively skewed for all injections. Pairwise two-sample Kolmogorov-Smirnov tests indicate that all cumulative distributions are significantly different from one another in each of WS01 and WS03 for all possible combinations of injections and watersheds (i.e., each cumulative distribution function is unique). While hyporheic flow path transit times were found to be largely insensitive to discharge (Figure 5d) [*Ward et al*., 2016], these results show that OLs are likely to change with discharge. However, as with transit times, changes in WS01 were larger than in WS03, providing further evidence that hyporheic flow paths are less variable in highly constrained valleys.

The ranges of possible flow path origination locations are constrained by the feasible bounds of θ, *K*, and *S*. These ranges in OLs generate corresponding ranges in all of the calculated length scales, timescales, and trends with discharge (supporting information Figures S11–S19). We found a range (i.e., the along-stream length of the feasible solutions in Figure 1b) averaging 17.6 m in WS01 (median 14.7 m, range 0.4–55.0 m) and averaging 34.7 m in WS03 (median 35.2 m, range 12.9–60.3 m). For the most narrowly defined ranges, the observed timescales limit the mathematically feasible solutions. For wells closer to the stream centerline, the observed timescales can be achieved for a wider range of θ, *K*, and *S*, indicating less certainty in the location of origination.

4.3. Discussion

4.3.1. Spatial and Temporal Dynamics of Transport Along Subsurface Flow Paths in the Stream Corridor

The distribution of potential OLs simulated by the model encompasses many channel morphologic features, not all of which will generate head gradients causing stream to riparian zone flux. Thus, if OLs change with stream discharge, they are unlikely to shift gradually, but rather, jump to new locations that are conducive to the generation of head gradients that favor flux from the stream to the subsurface (Figures 4c and 4d). Longer hyporheic flow path lengths under very low discharge could also result from more tortuous flow paths through the hyporheic zone as described by *Ward et al*. [2016]. In this case, down-valley transport would be controlled by the interaction between water table height and the structure and spatial heterogeneity of the colluvial materials filling the valley floor.

The potential flow path origination locations that can be detected at a given well defines a spatial window of detection (i.e., the along-stream origination locations from which flow paths will intersect the well). This is the spatial analog to the temporal window of detection defined by *Harvey et al*. [1996] and detailed in the literature [e.g., *Wagner and Harvey*, 1997; *Harvey and Wagner*, 2000; *Ward et al*., 2013a, 2013c]. Past studies focused on geomorphic units as drivers of exchange and other relatively small-scale features (see review by *Boano et al*. [2014]) have spatial windows of detection. As such, these studies were only sensitive to a suite of relatively short flow paths because near-stream well placement. In contrast, studies based on more extensive monitoring well networks [e.g., *Wondzell*, 2006; *Ward et al*., 2012; *Morrice et al*., 1997; *Wroblicky et al*., 1998] include a significantly larger spatial window of detection. The observation at a well is still subject to all temporal window of detection issues, where truncation of the observable breakthrough curve will necessarily limit interpretation [*Drummond et al*., 2012]. The spatial window of detection can be estimated using the hyporheic potential model to bound the spatial extent of the stream corridor that forms the support volume for a given observation in a monitoring well. Better constraining the spatial window of detection with the hyporheic potential model may reveal that flow paths originated further upstream than previously thought.

The importance of accurate hydraulic conductivity fields as a prerequisite to meaningful predictions of transport in stream corridors is broadly recognized. However, our results demonstrate that, even with the inherent uncertainty in hydrogeological parameters (θ, *K*, and *S* in this study), useful information about connectivity dynamics can be assessed. While we considered values of *K* potentially spanning orders of magnitude, the resultant spatial and temporal metrics do not show the same degree of variability (Figure 5). This

result is because the hydrogeologic properties are one control on the metrics, but in many cases the range is also bounded by the geometry of the problem and the observed timescales of the stream and hyporheic flow paths. As such, meaningful information and reasonably narrow bounds on transport metrics may be estimated, even with high uncertainty in site-specific parameter values.

4.3.2. A Revised Conceptual Model of the Stream Corridor in Steep, Confined Valley Bottoms

One key finding of this study is that subsurface flow paths increase in length during lower-discharge conditions. One common explanation for this is that cross-valley hydraulic gradients toward the stream relax through base flow recession, enabling expansion of the hyporheic zone and more rapid downwelling from the stream to the hyporheic and riparian zones [e.g., *Harvey et al.*, 1996; *Wondzell and Swanson*, 1996]. However, *Voltz et al.* [2013] demonstrate that cross-valley gradients are both small and relatively static through base flow recession in this system. Furthermore, observation of hyporheic extent as judged by solute tracer presence in the monitoring well network and riparian zone indicates the hyporheic zone remains equally extensive throughout base flow recession [*Wondzell*, 2006; *Ward et al.*, 2012, 2014]. On this basis, the explanation of cross-valley gradient or hydraulic constraint is not correct for the highly constrained, steep valley bottoms of this study. Rather, we attribute origination occurring farther upstream to be a result of the stream corridor structure. Our conceptual model is that for steep, confined valleys, the down-valley subsurface flow is relatively constant throughout the season. All discharge in excess of down-valley subsurface capacity is transported by the stream [*Wondzell and Gooseff*, 2013; *Ward et al.*, 2016]. This is analogous to saturation excess overland flow. Under high-discharge conditions, the valley bottom is already near capacity, so the introduced tracer is transported preferentially in the stream. Under low-discharge conditions, the valley bottom has excess capacity. The tracer introduced into the stream rapidly downwells because there is down-valley transport capacity in the subsurface. Under this conceptual model, the stream becomes largely an "overflow," providing transport when the down-valley discharge exceeds what can be accommodated in the subsurface. Therefore, valley characteristics are the key controls on transport and connectivity. Stream morphology, then, is important for local-scale exchanges but likely not dominant for valley-scale exchange, as demonstrated by the lack of correlation we see between stream form and predicted OLs (Figure 6).

4.3.3. Management Implications for Time-Variable Connectivity in the Stream Corridor

The sustainable management of river corridors is a growing area of interest [e.g., *Budd et al.*, 1987; *Kannel et al.*, 2008; *Kline and Cahoon*, 2010; *Biron et al.*, 2014; *Buffin-Bélanger et al.*, 2015]. In mountain streams,

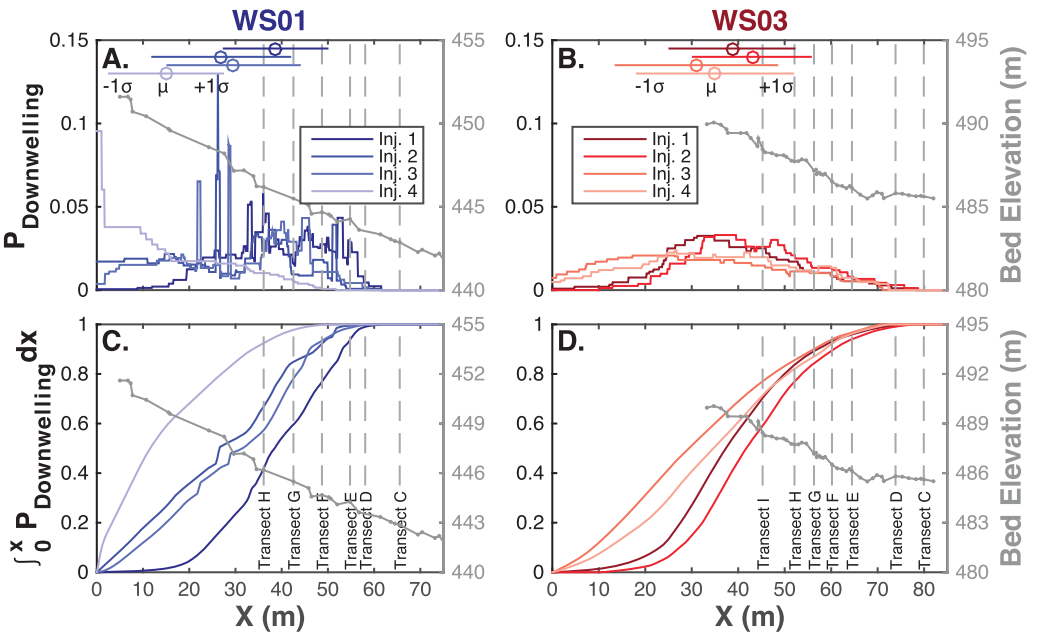

Figure 6. (a, b) Probability of flow path origination along the stream for each watershed and injection. Mean and standard deviations for each injection are shown along the top of each figure. (c, d) Cumulative distribution of origination probability. The streambed topography is shown in light gray, associated with the right-hand *y* axis on each plot. Finally, well transect locations are indicated by the dashed vertical lines.

extensive effort has focused on the management of sediment and large woody debris and sediment in the river corridor which promote exchange in the stream corridor [e.g., *Wohl*, 2004; *Wohl et al*., 2017]. One motivation for recent interest is the proposed Clean Water Rule [*US DoD and US EPA*, 2015] that clarifies hyporheic and riparian zones (i.e., stream corridors) are germane to the physical, chemical, and biological functions of streams. Consequently, stream corridors are clarified to fall within the scope of the Clean Water Act [*US EPA*, 2015], with stream corridor management designed to maintain the physical, chemical, and biological health of the stream given the well-known ecosystem services associated with connectivity (see reviews by *Brunke and Gonser* [1997], *Boulton et al*. [1998], *Krause et al*. [2011], *Merill and Tonjes* [2014], and *Ward* [2016]).

Management of stream corridors remains difficult because connectivity between surface and subsurface waters and the associated ecological functions are known to be spatially variable and temporally dynamic [*Vidon et al*., 2010; *Jencso et al*., 2009, 2010; *Jencso and McGlynn*, 2011; *Pringle*, 2003; *Bracken and Croke*, 2007; *Tetzlaff et al*., 2007; *Blume and Van Meerveld*, 2015; *Wainwright et al*., 2011]. Design of sound management strategies requires an understanding of both spatial and temporal dimensions of connectivity between streams and their corridors. The holistic management of entire stream corridors, rather than just the streams themselves, is of growing importance because many of the ecological functions rivers provide occur primarily along subsurface flow paths [*Harvey and Gooseff*, 2015].

Based on our study of steep, narrow, constrained headwater stream corridors, we outline how connectivity in the stream corridor could be considered by resource managers for these types of systems. For cases where flow path geometry is time-invariant (as we hypothesized), identification of the connected locations could be conducted under any discharge. On this basis, connectivity is readily established and the Clean Water Act could be applied to the stream corridor as proposed in the Clean Water Rule [*US DoD and US EPA*, 2015; *US EPA*, 2015]. However, we found that flow path geometry was dynamic through base flow recession (contrary to our hypothesis), even for flow paths where hyporheic transport timescales were not significantly different between experiments (e.g., WS03, near-stream locations in WS01). In many cases, hyporheic flow paths may originate immediately at the injection location ($X = 0$, Figure 6), suggesting that some flow paths originating upstream of the injection location were also intersecting the wells. Given this length of down-valley subsurface transport, the extensive flow path networks that span nearly the entire valley bottom at the field site [*Wondzell*, 2006; *Wondzell et al*., 2009; *Voltz et al*., 2013; *Ward et al*., 2016], and the dynamics of the flow paths themselves, identification of a fixed location for management would be difficult. Instead, a strategy of managing the stream corridor in its entirety would be more appropriate [*Hester and Gooseff*, 2010, 2011; *Harvey and Gooseff*, 2015]. Still, this management strategy presents a logistical challenge, particularly where the stream or river corridor serves also serves as a corridor for infrastructure and transportation, or where extensive human activity including agriculture, silviculture, and/or urbanization are present.

Finally, we acknowledge here that our conclusions are based on study of a specific type of stream corridor (steep, narrow, and confined). The relationships between valley morphology, discharge, and connectivity observed in this study—and therefore the recommendations based on them—may not hold in other systems (e.g., low-gradient rivers in large alluvial floodplains). Still, we contend the HPM provides one way to characterize connectivity in a stream or river corridor.

5. Conclusions

The hyporheic potential model, as derived, validated, and applied in this study, provides a reduced complexity model to relate transport times in the stream corridor to flow path geometry. This linkage provides a spatial dimension that has been heretofore lacking from many solute tracer studies. We acknowledge that the HPM includes several assumptions in its application. The key remaining uncertainty in the model application is the subsurface hydrogeologic structure (e.g., hydraulic conductivity and porosity fields). Still, the hyporheic potential model is the first tool to predict flow path geometry in stream corridors. Furthermore, the reduced complexity model has relatively modest data requirements, allowing for rapid application as a forward model to rapidly assess a system of interest or plan for a more detailed field campaign.

In this study, we asked where flow paths originate from the stream channel. We found that most flow paths originated upstream of the study well network, which was not expected based on our visual inspection of

the site. By narrowing the ranges of θ, K, and S it is possible that these origination ranges could be better constrained. Next, we asked if origination location was dynamic as a function of in-stream discharge. We hypothesized that flow path geometry would be stable through base flow recession given relatively constant transit times observed in empirical studies. Instead, despite relatively constant transit times, we found that flow path origination locations systematically shift in the upstream direction in both WS01 and WS03 with decreasing in-stream discharge. Moreover, we found general trends that hyporheic transport represents an increasing fraction of total transport length as discharge decreases. We demonstrate that the relatively simple hyporheic potential model detailed in this study could be used to rapidly assess the connectivity of streams with their hyporheic zones, riparian zones, and floodplains with basic valley bottom information. The hyporheic potential model or the finite element model presented here could also be applied in a forward modeling application to plan an experiment or field campaign.

Acknowledgments

Data and facilities were provided by the H.J. Andrews Experimental Forest research program, funded by the National Science Foundation's (NSF's) Long-Term Ecological Research Program (DEB 1440409), US Forest Service Pacific Northwest Research Station, and Oregon State University. M. N. Gooseff, K. Singha, and A. S. Ward were supported by the NSF's Hydrologic Sciences program, under grant EAR 0911435. Wondzell was supported by NSF grant EAR 1417603. Tools for solute tracer time series analyses and spatial data processing were developed by Ward and others with support provided in part by NSF grant EAR 1505309 and EAR 1331906 for the Critical Zone Observatory for Intensively Managed Landscapes (IML-CZO), a multi-institutional collaborative effort. A. S. Ward was also supported by the Indiana University Office of the Vice Provost for Research. Any opinions, findings, and conclusions or recommendations expressed in this material are those of the authors and do not necessarily reflect the views of the National Science Foundation, U.S. Forest Service, or Indiana University. Precipitation and discharge data are available from the H.J. Andrews Experimental Forest Data catalog (http://andrewsforest.oregonstate.edu/). Topographic survey, in-stream-specific conductance, and downwell-specific conductance data are available upon request to the corresponding author. The authors declare no conflicts of interest.

References

Bencala, K. E., M. N. Gooseff, and B. A. Kimball (2011), Rethinking hyporheic flow and transient storage to advance understanding of stream-catchment connections, *Water Resour. Res.*, *47*, W00H03, doi:10.1029/2010WR010066.

Beven, K. J. (1993), Prophecy, reality and uncertainty in distributed hydrological modelling, *Adv. Water Resour.*, *16*(1), 41–51, doi:10.1016/0309-1708(93)90028-E.

Beven, K. J. (2006), A manifesto for the equifinality thesis, *J. Hydrol.*, *320*(1–2), 18–36.

Biron, P. M., T. Buffin-Bélanger, M. Larocque, G. Choné, C. A. Cloutier, M. A. Ouellet, S. Demers, T. Olsen, C. Desjarlais, and J. Eyquem (2014), Freedom space for rivers: A sustainable management approach to enhance river resilience, *Environ. Manage.*, *54*(5), 1056–1073, doi:10.1007/s00267-014-0366-z.

Blume, T., and H. J. Van Meerveld (2015), From hillslope to stream: Methods to investigate subsurface connectivity, *WIREs Water*, *2*(3), 177–198.

Boano, F., J. W. Harvey, A. Marion, A. I. Packman, R. Revelli, L. Ridolfi, and A. Worman (2014), Hyporheic flow and transport processes: Mechanisms, models, and biogeochemical implications, *Rev. Geophys.*, *52*, 603–679, doi:10.1002/2012RG000417.

Boulton, A. J., S. Findlay, P. Marmonier, E. H. Stanley, and H. M. Valett (1998), The functional significance of the hyporheic zone in streams and rivers, *Annu. Rev. Ecol. Syst.*, *29*(1), 59–81.

Bracken, L. J., and J. Croke (2007), The concept of hydrological connectivity and its contribution to understanding runoff-dominated geomorphic systems, *Hydrol. Processes*, *21*(13), 1749–1763.

Brunke, M., and T. Gonser (1997), The ecological significance of exchange processes between rivers and groundwater, *Freshwater Biol.*, *37*, 1–33.

Budd, W. W., P. L. Cohen, P. R. Saunders, and F. R. Steiner (1987), Stream corridor management in the Pacific Northwest: I. Determination of stream-corridor widths, *Environ. Manage.*, *11*(5), 587–597, doi:10.1007/BF01880157.

Buffin-Bélanger, T., P. M. Biron, M. Larocque, S. Demers, T. Olsen, G. Choné, M. A. Ouellet, C. A. Cloutier, C. Desjarlais, and J. Eyquem (2015), Freedom space for rivers: An economically viable river management concept in a changing climate, *Geomorphology*, *251*, 137–148, doi:10.1016/j.geomorph.2015.05.013.

Cardenas, M. B. (2008a), The effect of river bend morphology on flow and timescales of surface water-groundwater exchange across point-bars, *J. Hydrol.*, *362*(1), 134–141.

Cardenas, M. B. (2008b), Surface water-groundwater interface geomorphology leads to scaling of residence times, *Geophys. Res. Lett.*, *35*, L08402, doi:10.1029/2008GL033753.

Cardenas, M. B., and V. A. Zlotnik (2003), Three-dimensional model of modern channel bend deposits, *Water Resour. Res.*, *39*(6), 1141, doi:10.1029/2002WR001383.

Covino, T. P., B. L. McGlynn, and J. Mallard (2011), Stream-groundwater exchange and hydrologic turnover at the network scale, *Water Resour. Res.*, *47*, W12521, doi:10.1029/2011WR010942.

Drummond, J. D., T. P. Covino, A. F. Aubeneau, D. Leong, S. Patil, R. Schumer, and A. I. Packman (2012), Effects of solute breakthrough curve tail truncation on transit time estimates: A synthesis of solute tracer injection studies, *J. Geophys. Res.*, *117*, G00N08, doi:10.1029/2012JG002019.

Dyrness, C. T. (1969), Hydrologic properties of soils on three small watersheds in the western Cascades of Oregon, *Res. Pap. PNW-111*, 17 p., U.S. Dep. of Agric. For. Serv., Portland, Oreg.

FISRWG (Federal Interagency Stream Restoration Working Group) (1998), *Stream Corridor Restoration: Principles, Processes, and Practices, GPO Item No. 0120-A*, Federal Interagency Stream Restoration Working Group, Washington, D. C.

Gooseff, M. N. (2010), Defining hyporheic zones-advancing our conceptual and operational definitions of where stream water and groundwater meet, *Geogr. Compass*, *4*(8), 945–955.

Gooseff, M. N., J. K. Anderson, S. M. Wondzell, J. LaNier, and R. Haggerty (2006), A modelling study of hyporheic exchange pattern and the sequence, size, and spacing of stream bedforms in mountain stream networks, Oregon, USA, *Hydrol. Processes*, *20*(11), 2443–2457.

Harms, T. K., and N. B. Grimm (2008), Hot spots and hot moments of carbon and nitrogen dynamics in a semiarid riparian zone, *J. Geophys. Res.*, *113*, G01020, doi:10.1029/2007JG000588.

Harvey, J., and M. Gooseff (2015), River corridor science: Hydrologic exchange and ecological consequences from bedforms to basins, *Water Resour. Res.*, *51*, 6893–6922, doi:10.1002/2015WR017617.

Harvey, J. W., and B. J. Wagner (2000), Quantifying hydrologic interactions between streams and their subsurface hyporheic zones, in *Streams and Ground Waters*, edited by J. B. Jones and P. J. Mulholland, pp. 3–44, Academic Press, San Diego, Calif.

Harvey, J. W., B. J. Wagner, and K. E. Bencala (1996), Evaluating the reliability of the stream tracer approach to characterize stream-subsurface water exchange, *Water Resour. Res.*, *32*(8), 2441–2451.

Hester, E. T., and M. N. Gooseff (2010), Moving beyond the banks: Hyporheic restoration is fundamental to restoring ecological services and functions of streams, *Environ. Sci. Technol.*, *44*(5), 1521–1525.

Hester, E. T., and M. N. Gooseff (2011), Hyporheic restoration in streams and rivers, in *Stream Restoration in Dynamic Fluvial Systems: Scientific Approaches, Analyses, and Tools, Geophys. Monogr. Ser.*, vol. 194, edited by A. Simon, S. J. Bennett, and J. M. Castro, pp. 167–187, AGU, Washington, D. C.

Irvine, D. J., and L. K. Lautz (2015), High resolution mapping of hyporheic fluxes using streambed temperatures: Recommendations and limitations, *J. Hydrol.*, *524*, 137–146.
Irvine, D. J., R. H. Cranswick, C. T. Simmons, M. A. Shanafield, and L. K. Lautz (2015), The effect of streambed heterogeneity on groundwater-surface water exchange fluxes inferred from temperature time series, *Water Resour. Res.*, *51*, 198–212, doi:10.1002/2014WR015769.
Jencso, K. G., and B. L. McGlynn (2011), Hierarchical controls on runoff generation: Topographically driven hydrologic connectivity, geology, and vegetation, *Water Resour. Res.*, *47*, W11527, doi:10.1029/2011WR010666.
Jencso, K. G., B. L. McGlynn, M. N. Gooseff, S. M. Wondzell, K. E. Bencala, and L. A. Marshall (2009), Hydrologic connectivity between landscapes and streams: Transferring reach-and plot-scale understanding to the catchment scale, *Water Resour. Res.*, *45*, W04428, doi:10.1029/2008WR007225.
Jencso, K. G., B. L. McGlynn, M. N. Gooseff, K. E. Bencala, and S. M. Wondzell (2010), Hillslope hydrologic connectivity controls riparian groundwater turnover: Implications of catchment structure for riparian buffering and stream water sources, *Water Resour. Res.*, *46*, W10524, doi:10.1029/2009WR008818.
Kannel, P. R., S. Lee, and Y. S. Lee (2008), Assessment of spatial-temporal patterns of surface and ground water qualities and factors influencing management strategy of groundwater system in an urban river corridor of Nepal, *J. Environ. Manage.*, *86*(4), 595–604, doi:10.1016/j.jenvman.2006.12.021.
Kasahara, T., and S. M. Wondzell (2003), Geomorphic controls on hyporheic exchange flow in mountain streams, *Water Resour. Res.*, *39*(1), 1005, doi:10.1029/2002WR001386.
Kline, M., and B. Cahoon (2010), Protecting river corridors in Vermont, *J. Am. Water Resour. Assoc.*, *46*(2), 227–236, doi:10.1111/j.1752-1688.2010.00417.x.
Krause, S., D. M. Hannah, J. H. Fleckenstein, C. M. Heppell, D. Kaeser, R. Pickup, G. Pinay, A. L. Robertson, and P. J. Wood (2011), Inter-disciplinary perspectives on processes in the hyporheic zone, *Ecohydrology*, *4*(4), 481–499.
Malzone, J. M., C. S. Lowry, and A. S. Ward (2016), Response of the hyporheic zone to transient groundwater fluctuations on the annual and storm event time scales, *Water Resour. Res.*, *52*, 5301–5321, doi:10.1002/2014WR015716.
McGuire, K. J., and J. J. McDonnell (2010), Hydrological connectivity of hillslopes and streams: Characteristic time scales and nonlinearities, *Water Resour. Res.*, *46*, W10543, doi:10.1029/2010WR009341.
Menichino, G. T., A. S. Ward, and E. T. Hester (2014), Macropores as preferential flow paths in meander bends, *Hydrol. Processes*, *28*(3), 482–495, doi:10.1002/hyp.9573.
Merill, L., and D. J. Tonjes (2014), A review of the hyporheic zone, stream restoration, and means to enhance denitrification, *Crit. Rev. Environ. Sci. Technol.*, *44*(21), 2337–2379, doi:10.1080/10643389.2013.829769.
Morrice, J. A., H. Valett, C. N. Dahm, and M. E Campana (1997), Alluvial characteristics, groundwater-surface water exchange and hydrological retention in headwater streams, *Hydrol. Processes*, *11*(3), 253–267.
Ocampo, C. J., M. Sivapalan, and C. Oldham (2006), Hydrological connectivity of upland-riparian zones in agricultural catchments: Implications for runoff generation and nitrate transport, *J. Hydrol.*, *331*(3), 643–658.
Oreskes, N., K. Shrader-Frechette, and K. Belitz (1994), Verification, validation, and confirmation of numerical models in the Earth sciences, *Science*, *263*, 641–646.
Payn, R. A., M. N. Gooseff, B. L. McGlynn, K. E. Bencala, and S. M. Wondzell (2009), Channel water balance and exchange with subsurface flow along a mountain headwater stream in Montana, United States, *Water Resour. Res.*, *45*, W11427, doi:10.1029/2008WR007644.
Payn, R. A., M. N. Gooseff, B. L. McGlynn, K. E. Bencala, and S. M. Wondzell (2012), Exploring changes in the spatial distribution of stream baseflow generation during a seasonal recession, *Water Resour. Res.*, *48*, W04519, doi:10.1029/2011WR011552.
Poeter, E. (2007), All models are wrong, how do we know which are useful?, *Ground Water*, *45*(4), 390–391, doi:10.1111/j.1745-6584.2007.00350.x.
Pringle, C. (2003), What is hydrologic connectivity and why is it ecologically important?, *Hydrol. Processes*, *17*(13), 2685–2689.
Schmadel, N. M., A. S. Ward, C. S. Lowry, and J. M. Malzone (2016), Hyporheic exchange controlled by dynamic hydrologic boundary conditions, *Geophys. Res. Lett.*, *43*, 4408–4417, doi:10.1002/2016GL068286.
Stanford, J. A., and Ward, J. V. (1993), An ecosystem perspective of alluvial rivers: Connectivity and the hyporheic corridor, *J. North Am. Benthol. Soc.*, *12*, 48–60.
Swanson, F. J., and M. E. James (1975), Geology and Geomorphology of the H.J. Andrews Experimental Forest, Western Cascades, Oregon, Publ. 484, 14 p., U.S. Dep. of Agric., Portland, Oreg.
Swanson, F. J., and J. A. Jones (2002), Geomorphology and hydrology of the H.J. Andrews Experimental Forest, Blue River, Oregon, in *Field Guide to Geologic Processes in Cascadia*, Oregon Department of Geology and Mineral Industries, Special Paper 36, edited by G.W. Moore, pp. 288–314, Nature of the Northwest Information Center, Portland, Oreg.
Tetzlaff, D., C. Soulsby, P. J. Bacon, A. F. Youngson, C. Gibbins, and I. A. Malcolm (2007), Connectivity between landscapes and river-scapes—A unifying theme in integrating hydrology and ecology in catchment science?, *Hydrol. Processes*, *21*(10), 1385–1389.
US DoD and US EPA (2015), Clean water rule: Definition of "waters of the United States," *Fed. Regist.*, *80*(124), 37,054–37,127.
US EPA (2015), Connectivity of streams & wetlands to downstream waters: A review and synthesis of the scientific evidence, final report EPA/600/R-14/475F, Washington, D. C.
Vidon, P. G., et al. (2010), Hot spots and hot moments in riparian zones: Potential for improved water quality management, *J. Am. Water Resour. Assoc.*, *46*(2), 278–298.
Voltz, T. J., M. N. Gooseff, A. S. Ward, K. Singha, M. Fitzgerald, and T. Wagener (2013), Riparian hydraulic gradient and stream-groundwater exchange dynamics in steep headwater valleys, *J. Geophys. Res. Earth Surf.*, *118*, 953–969, doi:10.1002/jgrf.20074.
Wagner, B. J., and J. W. Harvey (1997), Experimental design for estimating parameters of rate-limited mass transfer: Analysis of stream tracer studies, *Water Resour. Res.*, *33*(7), 1731–1741.
Wainwright, J., L. Turnbull, T. G. Ibrahim, I. Lexartza-Artza, S. F. Thornton, and R. E. Brazier (2011), Linking environmental regimes, space and time: Interpretations of structural and functional connectivity, *Geomorphology*, *126*(3), 387–404.
Ward, A. S. (2016), The evolution and state of interdisciplinary hyporheic research, *WIREs Water*, *3*(1), 83–103, doi:10.1002/wat2.1120.
Ward, A. S., M. N. Gooseff, and P. A. Johnson (2011), How can subsurface modifications to hydraulic conductivity be designed as stream restoration structures? Analysis of Vaux's conceptual models to enhance hyporheic exchange, *Water Resour. Res.*, *47*, W08512, doi:10.1029/2010WR010028.
Ward, A. S., M. Fitzgerald, M. N. Gooseff, T. J. Voltz, A. M. Binley, and K. Singha (2012), Hydrologic and geomorphic controls on hyporheic exchange during base flow recession in a headwater mountain stream, *Water Resour. Res.*, *48*, W04513, doi:10.1029/2011WR011461.
Ward, A. S., M. N. Gooseff, T. J. Voltz, M. Fitzgerald, K. Singha, and J. P. Zarnetske (2013a), How does rapidly changing discharge during storm events affect transient storage and channel water balance in a headwater mountain stream?, *Water Resour. Res.*, *49*, 5473–5486, doi:10.1002/wrcr.20434.

Ward, A. S., M. N. Gooseff, and K. Singha (2013b), How does subsurface characterization affect simulations of hyporheic exchange?, *Ground Water*, *51*(1), 14–28, doi:10.1111/j.1745-6584.2012.00911.x.

Ward, A. S., R. A. Payn, M. N. Gooseff, B. L. McGlynn, K. E. Bencala, C. A. Kelleher, S. M. Wondzell, and T. Wagener (2013c), Variations in surface water-ground water interactions along a headwater mountain stream: Comparisons between transient storage and water balance analyses, *Water Resour. Res.*, *49*, 3359–3374, doi:10.1002/wrcr.20148.

Ward, A. S., M. N. Gooseff, M. Fitzgerald, T. J. Voltz, and K. Singha (2014), Spatially distributed characterization of hyporheic solute transport during baseflow recession in a headwater mountain stream using electrical geophysical imaging, *J. Hydrol.*, *517*, 362–377, doi:10.1016/j.jhydrol.2014.05.036.

Ward, A. S., N. M. Schmadel, S. M. Wondzell, C. J. Harman, M. N. Gooseff, and K. Singha (2016), Hydrogeomorphic controls on hyporheic and riparian transport in two headwater mountain streams during base flow recession, *Water Resour. Res.*, *52*, 1479–1497, doi:10.1002/2015WR018225.

Wohl, E. (2014), *Rivers in the Landscape: Science and Management*, 336 p., John Wiley, Hoboken, N. J.

Wohl, E., F. J. Magilligan, and S. L. Rathburn (2017), Introduction to the special issue: Connectivity in geomorphology, *Geomorphology*, *277*, 1–5, doi:10.1016/j.geomorph.2016.11.005.

Wondzell, S. M. (2006), Effect of morphology and discharge on hyporheic exchange flows in two small streams in the Cascade Mountains of Oregon, USA, *Hydrol. Processes*, *20*(2), 267–287.

Wondzell, S. M., and M. N. Gooseff (2013), Geomorphic controls on hyporheic exchange across scales: Watersheds to particles, in *Treatise on Geomorphology*, vol. 9, edited by J. Schroder and E. Wohl, pp. 203–218, Academic, San Diego, Calif.

Wondzell, S. M., and F. J. Swanson (1996), Seasonal and storm dynamics of the hyporheic zone of a 4th-order mountain stream. 1: Hydrologic processes, *J. North Am. Benthol. Soc.*, *15*(1), 3–19.

Wondzell, S. M., and F. J. Swanson (1999), Floods, channel change, and the hyporheic zone, *Water Resour. Res.*, *35*(2), 555–567.

Wondzell, S. M., J. LaNier, and R. Haggerty (2009), Evaluation of alternative groundwater flow models for simulating hyporheic exchange in a small mountain stream, *J. Hydrol.*, *364*(1–2), 142–151.

Wroblicky, G. J., M. E. Campana, H. M. Valett, and C. N. Dahm (1998), Seasonal variation in surface-subsurface water exchange and lateral hyporheic area of two stream-aquifer systems, *Water Resour. Res.*, *34*(3), 317–328.

Zarnetske, J. P., R. Haggerty, S. M. Wondzell, V. A. Bokil, and R. González-Pinzón (2012), Coupled transport and reaction kinetics control the nitrate source-sink function of hyporheic zones, *Water Resour. Res.*, *48*, W11508, doi:10.1029/2012WR011894.